JOURNAL OF SOLID STATE CHEMISTRY 64, 47–56 (1986)

Crystal Structure of $Li_{0.33}MoO_3$, a Stoichiometric, Triclinic, Lithium Molybdenum Bronze

P. P. TSAI, J. A. POTENZA, M. GREENBLATT, AND H. J. SCHUGAR

Department of Chemistry, Rutgers, The State University of New Jersey, New Brunswick, New Jersey 08903

Received December 16, 1985

The crystal structure of $Li_{0.33}MoO_3$, the first structurally well-characterized triclinic bronze, has been determined from single-crystal X-ray diffraction data. $Li_{0.33}MoO_3$ crystallizes in space group $P\bar{1}$ with $a = 13.079(2)$, $b = 15.453(2)$, $c = 7.476(1)$ Å, $\alpha = 96.97(2)$, $\beta = 106.56(2)$, $\gamma = 103.368(9)°$, $Z = 24$, and $R_F = 0.032$ for 10,664 reflections with $F_o^2 \geq 3\sigma(F_o^2)$. Distorted lithium and molybdenum octahedra form V_2O_5-type layers parallel to the *ac* plane. Each layer contains six unique MoO_6 units and two unique LiO_6 units. Four such layers, two of which are unique, are interconnected through edge and corner sharing to form a three-dimensional network structure. The location of lithium atoms at completely occupied octahedral sites establishes the stoichiometric composition $LiMo_3O_9$. Examination of the structure suggests that $Li_{0.33}MoO_3$ should be a semiconductor except along *c* where metallic conduction is possible.

Introduction

Because of their interesting structural and electrical properties, the molybdenum oxide bronzes, M_xMoO_3, have attracted considerable attention. Several materials for which *M* is a group IA metal have been prepared and characterized. The potassium blue bronze $K_{0.3}MoO_3$ is a quasi-one-dimensional metallic conductor and undergoes a charge-density wave-driven phase transition at 180 K (*1*). A recent redetermination of the structure of the $Cs_{0.33}MoO_3$ red bronze (*2*) shows that is it isostructural with the $K_{0.33}MoO_3$ analog (*3*). These bronzes are semiconducting (*4, 5*) at room temperature despite the similarity of their structure to that of $K_{0.3}MoO_3$ (*6*).

Single crystals of the blue bronze Li_xMoO_3 ($0.31 \leq x \leq 0.39$) were first prepared by Reau *et al.* (*7*). According to their study, this material crystallized in the monoclinic system with $a = 24.54(5)$, $b = 7.450(6)$, $c = 15.11(4)$ Å, and $\beta = 106° \pm 5'$. Later, Greenblatt and co-workers prepared single crystals of $Li_{0.33}MoO_3$ using electrolysis (*5, 8*) and temperature gradient flux (*9*) techniques. Three crystal habits (needles, prisms, and plates) were observed and the range of composition noted by Reau *et al.* was not reproduced. Crystals obtained by electrolysis at 560°C (*5*) typically were twinned and were characterized as monoclinic with cell dimensions similar to those reported by Reau *et al.* (*7*), whereas crystals grown by the gradient flux technique could not be indexed uniquely using monoclinic symmetry. Physical properties were also reported (*5*), but on poor quality, twinned, and very small crystals. $Li_{0.33}$

0022-4596/86 $3.00

TABLE I

CRYSTAL AND REFINEMENT DATA FOR $Li_{0.33}MoO_3$

fw	146.23
a, Å	13.079(2)
b, Å	15.453(2)
c, Å	7.476(1)
α, deg	96.97(2)
β, deg	106.56(2)
γ, deg	103.368(9)
V, Å^3	1380.4(9)
Space group	$P\bar{1}$
Z	24
No. of reflcns used to determine cell constants	25 ($22.95 \leq \theta \leq 30.48$)
d_{calcd}, g/cm^3	4.22
d_{obsd}, g/cm^3	4.21(7)
λ(Mo$K\alpha$), Å	0.71073
Monochromator	Graphite
Linear abs coeff, cm^{-1}	52.6
Cryst dimens, mm	0.12 × 0.15 × 0.58
Relative transmission factor range	0.90–1.00
Diffractometer	Enraf-Nonius CAD-4
Data collection method	θ–2θ
2θ range, deg	2–70
Temp, K	296(1)
Scan range, deg	$1.0 + 0.35 \tan \theta$
No. of std reflcns	3
% variation in std intens	±0.25
No of unique data collected	12,095
No. of data used in refinement ($F_o^2 \geq 3\sigma F_o^2$)	10,664
Data: parameter ratio	42.0
Final GOF[a]	1.92
Final R_F[b]	0.032
Final R_{wF}[c]	0.055
Weighting scheme[d]	$w = 4F_o^2/\sigma^2(F_o^2)$
Systematic absences observed	None
Data collected	$h \pm k \pm l$
Final largest shift/esd	0.07
Highest peak in final difference map, e/Å^3	2.5

[a] GOF: Esd of an observation of unit weight.

[b] $R_F = \Sigma||F_o| - |F_c||/\Sigma|F_o|$.

[c] $R_{wF} = (\Sigma w(|F_o| - |F_c|)^2/\Sigma w F_o^2)^{1/2}$.

[d] $\sigma(F_o^2) = [S^2(C + R^2B) + (PF_o^2)^2]^{1/2}Lp$ where S is the scan rate, C is the total integrated peak count, R is the ratio of scan time to background counting time, B is the total background count, Lp is the Lorentz-polarization factor, and P is an experimental instability factor introduced to downweight intense reflections (P = 0.04 in this case).

MoO_3 was found to be a semiconductor with a room temperature resistivity of ~5 Ω cm (*5*).

To help understand the structural/physical property relationships in this system, a single-crystal X-ray diffraction study was undertaken on a prismatic crystal from the temperature gradient preparation (*9*). To our surprise, the crystal was triclinic. No triclinic molybdenum bronze has been observed previously. Indeed, there is only one report of any transition metal bronze that may be triclinic. This system, sodium tungsten oxide, however, is not well characterized and may not be a single phase (*10*). We report here the structure of this unusual stoichiometric bronze; the results of transport property measurements on large single-crystal specimens will be reported elsewhere.

Experimental

X-ray crystallography. Large, prism shaped violet blue crystals of $Li_{0.33}MoO_3$ were prepared using a temperature gradient flux growth technique (*9*), and a single crystal 0.12 × 0.15 × 0.58 mm was mounted approximately along the c axis on a glass fiber. Details of the data collection process and structure solution are given in Table I. Diffractometer examination of the reciprocal lattice revealed a triclinic cell and no systematic absences. Successful solution and refinement of the structure fixed the space group as $P\bar{1}$. Intensity data were collected and corrected for Lorentz polarization, absorption (empirical), and decay effects.

The structure was solved by a combination of direct methods and difference Fourier techniques. The program MULTAN 82 (*11*) and the Enraf-Nonius Structure Determination Package (*12*) were used. Full-matrix least-squares refinement was based on F and neutral atom scattering factors were used. Anomalous dispersion

corrections were applied to the scattering factors of the Mo and O atoms. All Mo and O atoms were located from the initial E map and several difference Fourier maps. Refinement of the 12 unique Mo atoms (anisotropic) and 36 unique O atoms (isotropic) reduced R_F to 0.037. At this point, a difference map was prepared in an attempt to locate the 4 unique Li atoms in the asymmetric unit. The four largest peaks in the map (5.5–7.2 e/Å^3, next largest peak 2.5 e/Å^3) were located at positions which would complete distorted MO_6 octahedra, and were assigned as Li. Lithium atoms were added to the model and refined isotropically. All atoms, including lithium, refined smoothly. Several cycles of refinement with Mo atoms anisotropic and both O and Li atoms isotropic led to convergence (largest parameter shift = 0.07σ, where σ is the esd obtained from the inverse matrix) with $R_F = 0.032$ and $R_{wF} = 0.055$. Final atomic coordinates and isotropic thermal parameters are given in Table II. A final difference map revealed no unusual features. The largest peak was 2.54 e/Å^3 and was located 0.36 Å from O(12). To test the occupancy of the lithium sites, atom multipliers were refined while holding the isotropic temperature factors constant at their refined values. Refined lithium atom multipliers ranged from 0.95(2) to 1.05(2) (average 1.01(2)), indicating complete occupancy within experimental error. Further, we note that the average isotropic temperature factors show $\bar{B}_{iso}$(Li) > $\bar{B}_{eq}$(Mo) with the lighter metal having the higher temperature factors as might be expected. This effect has been observed previously with similar structures (*17, 18*); the $\bar{B}$(Li) and $\bar{B}$(Mo) values for the present structure (1.9(3), 0.61(8)) compare favorably with those for both the high- and low-temperature forms (1.7(4), 0.56(6) and 1.5(5), 0.71(6), respectively) of $Li_4Mo_4O_{13}$, which are structurally similar and which contain completely occupied sites. This provides further support for complete occupancy of the lithium sites in the present structure. Based on this evidence, we conclude that the structure is stoichiometric

TABLE II

FRACTIONAL ATOMIC COORDINATES AND THERMAL PARAMETERS

	x	y	z	B or B_{eq} (Å^2)
Mo(1)	−0.42950(2)	−0.10927(2)	0.38213(4)	0.777(4)
Mo(2)	0.35591(2)	−0.11749(2)	0.01822(3)	0.608(4)
Mo(3)	−0.14516(2)	−0.10903(2)	0.02645(4)	0.777(4)
Mo(4)	0.06374(2)	−0.11927(2)	0.38291(3)	0.594(4)
Mo(5)	−0.04765(2)	0.16427(2)	0.14080(3)	0.578(4)
Mo(6)	−0.34108(2)	0.16385(2)	0.49586(3)	0.591(4)
Mo(7)	−0.23986(2)	0.59883(2)	0.41142(3)	0.554(4)
Mo(8)	−0.03586(2)	0.60010(2)	0.25764(3)	0.555(4)
Mo(9)	−0.23984(2)	0.59644(2)	−0.10133(3)	0.527(4)
Mo(10)	−0.53360(2)	0.60115(2)	0.75167(3)	0.573(4)
Mo(11)	0.26420(2)	0.59709(2)	−0.09381(3)	0.536(4)
Mo(12)	−0.53429(2)	0.59914(2)	0.26373(3)	0.648(4)
O(1)	0.3681(2)	−0.1474(2)	0.7730(4)	1.22(4)*
O(2)	−0.4918(2)	−0.1413(2)	0.5666(3)	0.92(3)*
O(3)	0.2022(2)	−0.1427(2)	0.4614(4)	1.31(4)*
O(4)	0.3987(2)	−0.0074(2)	0.5794(4)	1.26(4)*
O(5)	−0.4878(2)	−0.2872(2)	0.3190(4)	1.34(4)*
O(6)	−0.4946(2)	−0.1432(2)	0.1193(3)	0.94(3)*
O(7)	0.2982(2)	−0.2879(2)	−0.0439(4)	1.13(3)*
O(8)	0.2014(2)	−0.1428(2)	−0.0798(4)	1.31(4)*
O(9)	−0.0949(2)	0.0078(2)	0.0818(4)	1.32(4)*
O(10)	−0.2153(2)	−0.2911(2)	−0.0560(4)	1.33(4)*
O(11)	−0.0314(2)	0.1467(2)	0.3944(4)	1.18(4)*
O(12)	−0.0583(2)	0.1383(2)	−0.1226(4)	1.67(4)*
O(13)	−0.0085(2)	0.2792(2)	0.1830(4)	1.30(4)*
O(14)	0.1050(2)	0.1438(2)	0.1827(4)	0.98(3)*
O(15)	−0.2850(2)	−0.1324(2)	−0.0483(4)	1.53(4)*
O(16)	0.1031(2)	0.1424(2)	0.7391(4)	0.98(3)*
O(17)	0.0068(2)	−0.2837(2)	0.3038(4)	1.17(3)*
O(18)	−0.1001(2)	0.0054(2)	0.5666(4)	1.30(4)*
O(19)	0.3050(2)	−0.2784(2)	0.4481(4)	1.41(4)*
O(20)	−0.3483(2)	0.1375(2)	0.7375(4)	1.81(4)*
O(21)	0.3045(2)	0.1332(2)	0.5616(4)	1.56(4)*
O(22)	0.3976(2)	−0.0038(2)	0.0617(4)	1.34(4)*
O(23)	−0.4500(2)	0.4256(2)	0.5061(3)	1.02(3)*
O(24)	−0.4314(2)	0.4149(2)	0.0136(3)	0.86(3)*
O(25)	0.4028(2)	0.4387(2)	0.1754(3)	0.73(3)*
O(26)	−0.4015(2)	0.5621(2)	0.3054(3)	0.80(3)*
O(27)	−0.2946(2)	0.4336(2)	−0.1561(3)	0.63(3)*
O(28)	−0.0880(2)	0.5835(2)	0.4683(3)	0.79(3)*
O(29)	0.2962(2)	0.5697(2)	0.6727(3)	0.80(3)
O(30)	−0.2269(2)	0.5662(2)	0.1547(3)	0.76(3)*
O(31)	0.1186(2)	0.5608(2)	−0.1776(3)	0.93(3)*
O(32)	−0.2161(2)	−0.2889(2)	0.4485(4)	1.42(4)*
O(33)	−0.2415(2)	0.5686(2)	0.6456(3)	1.00(3)*
O(34)	−0.0893(2)	0.5807(2)	−0.0141(3)	0.77(3)*
O(35)	0.0839(2)	0.5657(2)	0.3106(3)	1.05(3)*
O(36)	−0.5147(2)	0.2854(2)	0.2026(4)	1.29(4)*
Li(1)	−0.0308(5)	0.5872(5)	−0.245(1)	1.5(1)*
Li(2)	0.4457(6)	0.1379(5)	0.136(1)	1.9(1)*
Li(3)	−0.1508(6)	−0.1369(5)	0.518(1)	2.0(1)*
Li(4)	0.2427(6)	0.5897(5)	0.394(1)	2.1(1)*

Note. Starred atoms were refined isotropically, and the equivalent isotropic thermal parameter is given by $B_{eq} = 4(\Sigma_i\Sigma_j\beta_{ij}a_i \cdot a_j)/3$.

with empirical formula $LiMo_3O_9$. Lists of observed and calculated structure factors and anisotropic temperature factors are available.*

Results and Discussion

The chemical formula established by this structural determination is $LiMo_3O_9$. The structure can be viewed as derived from a ReO_3-type shear structure of V_2O_5-like layers (Fig. 1) (*13*) containing distorted MoO_6 and LiO_6 octahedra. A view of the structure along $\bar{b}^*$ (Fig. 2a) clearly shows a V_2O_5-like layer in the *ac* plane. In this layer, every fourth octahedron in the edge-shared zigzag chains contains lithium, and the chains are linked by corner sharing. The structure contains four such layers (Fig. 2b) parallel to the *ac* plane and interconnected by corner and edge sharing along b^* to form a three-dimensional network structure. Layers I and II, and II and III (Fig. 2b) are connected by corner sharing while layers III and IV are connected by edge sharing. Finally, layers IV and I′ are connected by corner sharing. Only two of the layers (e.g., II and III) are unique and are related centrosymmetrically to the remaining two.

Packing of the V_2O_5-like layers leads to channels through the structure. Along b^*, these are the size of one-quarter of the square-planar base of an octahedron (Fig. 2a). Along *c* (Fig. 2b), there are several channels, the largest of which is the size of the base of an octahedron. Channels exist in other directions (e.g., parallel to $a + c$), but none are as large as those parallel to *c*. We note that Fig. 2 is not completely realistic in the depiction of these channels because the ideal octahedra used in the model create regular cavities compared with those that actually exist in the structure.

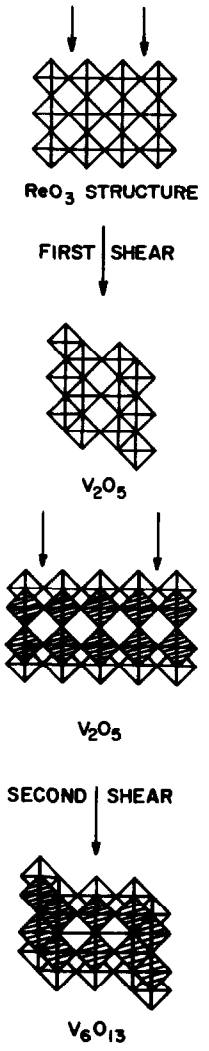

FIG. 1. Idealized V_2O_5 and V_6O_{13} structures derived by shearing the ReO_3 structure type along the planes indicated.

A view of the structure approximately along the b^* direction, showing the atom numbering scheme for the unique ions, is given in Fig. 3, while selected interatomic distances are listed in Table III (selected interatomic bond angles are listed in supplementary Table SII*). In the asymmetric unit, there are 12 crystallographically non-

* See NAPS document no. 04378 for 58 pages of supplementary material. Order from NAPS c/o Microfiche Publications, P.O. Box 3513, Grand Central Station, New York, N.Y. 10163. Remit in advance in U.S. funds only $19.15 for photocopies or $4.00 for microfiche. Outside the U.S. and Canada, add postage of $4.50 for the first 20 pages and $1.00 for each of 10 pages of material thereafter, $1.50 for microfiche postage.

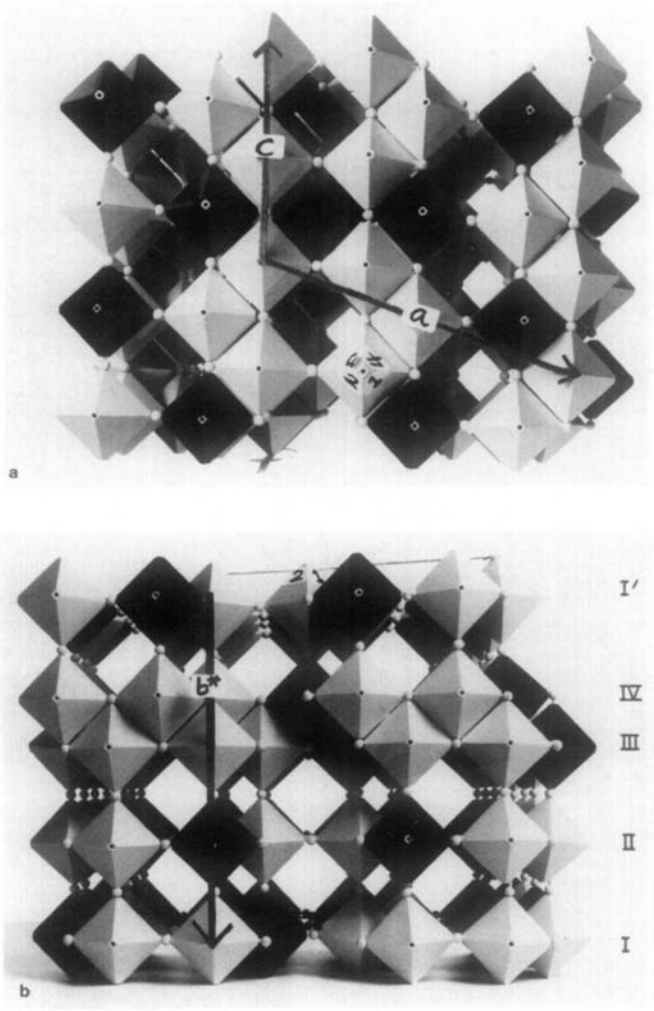

FIG. 2. (a) View along $\bar{b}^*$ of the $Li_{0.33}MoO_3$ structure built from idealized MoO_6 (light) and LiO_6 (dark) octahedra, and showing the V_2O_5-like planes. (b) View along c of the $Li_{0.33}MoO_3$ structure showing the V_2O_5-like layers connected along b^* (vertical direction) to form the three-dimensional structure.

equivalent molybdenum and 4 unique lithium ions, each associated with a distorted MO_6 octahedron. These octahedra all show similar orientations: for each octahedron, the three *trans* O · · · O vectors lie approximately along the b^*, c, and $[\bar{3}10]$ directions. Mo–O distances range from 1.663(2) to 2.710(2) Å while Li–O distances vary from 1.922(6) to 2.674(6) Å.

The Mo–O distances along $[\bar{3}10]$ show a large range (1.688(2)–2.710(2) Å) as do those along b^* (1.663(2)–2.684(2) Å) while those along c show a much smaller variation (1.861(2)–1.995(2) Å). *Cis* and *trans* O–Mo–O angles span the ranges 66.20(7)–107.30(9)° and 126.73(8)–178.49(9)°, respectively; corresponding values for the O–Li–O angles are 68.0(2)–109.3(3)° and 134.0(3)–177.8(4)°. Variations in Mo–O distances and O–Mo–O angles of this magni-

TABLE III

SELECTED INTERATOMIC DISTANCES[a] (Å) AND BOND VALENCE VALUES[b], *s*

Metal–oxygen distances

Mo–O octahedra

		s			*s*			*s*
Mo(1)–O(2)	1.852(2)	1.10	Mo(5)–O(8)	1.869(2)	1.04	Mo(9)–O(10)	1.666(2)	2.08
–O(4)	1.722(2)	1.70	–O(9)	2.306(2)	0.30	–O(25)	1.965(2)	0.77
–O(5)	2.622(2)	0.14	–O(11)	1.907(2)	0.92	–O(27)	2.400(2)	0.23
–O(6)	1.859(2)	1.08	–O(12)	1.920(2)	0.89	–O(30)	1.995(2)	0.70
–O(20)	2.697(2)	0.12	–O(13)	1.694(2)	1.88	–O(33)	1.882(2)	1.00
–O(21)	1.706(2)	1.80	–O(14)	2.036(2)	0.62	–O(34)	1.972(2)	0.76
Mo(2)–O(1)	1.897(2)	0.95	Mo(6)–O(1)	1.914(2)	0.90	Mo(10)–O(23)	1.861(2)	1.07
–O(6)	2.035(2)	0.63	–O(2)	2.036(2)	0.62	–O(24)	1.965(2)	0.77
–O(7)	2.510(2)	0.18	–O(3)	1.865(2)	1.06	–O(25)	1.908(2)	0.92
–O(8)	1.869(2)	1.04	–O(4)	2.306(2)	0.30	–O(26)	2.411(2)	0.23
–O(20)	1.915(2)	0.90	–O(19)	1.689(2)	1.91	–O(29)	2.055(2)	0.59
–O(22)	1.675(2)	2.01	–O(20)	1.923(2)	0.88	–O(36)	1.677(2)	2.00
Mo(3)–O(9)	1.726(2)	1.68	Mo(7)–O(26)	1.949(2)	0.81	Mo(11)–O(7)	1.696(2)	1.87
–O(10)	2.684(2)	0.12	–O(28)	1.986(2)	0.72	–O(24)	2.154(2)	0.44
–O(12)	2.710(2)	0.11	–O(29)	2.485(2)	0.19	–O(27)	1.938(2)	0.84
–O(14)	1.846(2)	1.12	–O(30)	1.990(2)	0.72	–O(29)	1.929(2)	0.86
–O(15)	1.688(2)	1.92	–O(32)	1.663(2)	2.10	–O(30)	2.417(2)	0.22
–O(16)	1.855(2)	1.09	–O(33)	1.871(2)	1.04	–O(31)	1.753(2)	1.53
Mo(4)–O(3)	1.872(2)	1.03	Mo(8)–O(17)	1.712(2)	1.76	Mo(12)–O(5)	1.678(2)	1.99
–O(11)	1.903(2)	0.94	–O(28)	1.909(2)	0.92	–O(23)	1.865(2)	1.06
–O(12)	1.912(2)	0.91	–O(30)	2.304(2)	0.30	–O(24)	1.966(2)	0.77
–O(16)	2.037(2)	0.62	–O(31)	2.396(2)	0.23	–O(25)	2.369(2)	0.25
–O(17)	2.423(2)	0.22	–O(34)	1.911(2)	0.91	–O(26)	1.906(2)	0.93
–O(18)	1.678(2)	1.99	–O(35)	1.725(2)	1.69	–O(27)	2.065(2)	0.57

Li–O octahedra

		s			*s*
Li(1)–O(13)	1.971(6)	0.24	Li(2)–O(1)	2.297(6)	0.12
–O(28)	2.047(6)	0.21	–O(2)	2.123(6)	0.18
–O(31)	2.023(6)	0.22	–O(6)	2.183(6)	0.16
–O(33)	2.577(6)	0.07	–O(15)	1.993(6)	0.23
–O(34)	2.085(6)	0.19	–O(22)	2.090(7)	0.19
–O(35)	2.251(6)	0.14	–O(36)	2.178(7)	0.16
Li(3)–O(11)	2.331(6)	0.12	Li(4)–O(19)	1.957(7)	0.25
–O(14)	2.170(7)	0.16	–O(23)	2.674(6)	0.06
–O(16)	2.181(7)	0.16	–O(27)	2.095(7)	0.19
–O(18)	2.097(7)	0.19	–O(29)	2.089(6)	0.19
–O(21)	1.943(6)	0.26	–O(33)	2.424(7)	0.10
–O(32)	2.246(7)	0.14	–O(35)	1.922(6)	0.27

Metal–metal distances

Mo–Mo edge-shared octahedra		Mo–Mo corner-shared octahedra	
Mo(1)–Mo(2)	3.2702(3)	Mo(2)–Mo(5)	3.7283(3)
Mo(1)–Mo(6)	3.3350(3)	Mo(2)–Mo(6)	3.7652(3)
Mo(3)–Mo(4)	3.2778(3)		3.8369(3)

TABLE III—*Continued*

Metal–metal distances			
Mo–Mo edge-shared octahedra		Mo–Mo corner-shared octahedra	
Mo(3)–Mo(5)	3.3451(3)	Mo(4)–Mo(5)	3.7647(3)
Mo(7)–Mo(8)	3.1895(3)		3.8304(3)
Mo(8)–Mo(9)	3.1837(3)	Mo(4)–Mo(6)	3.7264(3)
Mo(10)–Mo(11)	3.1648(3)	Mo(7)–Mo(9)	3.8304(3)
Mo(10)–Mo(12)	3.4098(3)		3.6484(3)
Mo(11)–Mo(12)	3.1651(3)	Mo(7)–Mo(12)	3.6921(3)
		Mo(9)–Mo(10)	3.7032(3)
		Mo(10)–Mo(12)	3.6428(3)
			3.8358(3)
Li–Mo edge-shared		Li–Mo corner-shared	
Li(1)–Mo(7)	3.231(5)	Li(1)–Mo(8)	3.762(5)
–Mo(9)	3.237(5)	–Mo(8)	3.730(5)
Li(1′)–Mo(8)	3.208(5)	–Mo(11)	3.658(5)
Li(2)–Mo(2)	3.186(6)	–Mo(5)	3.662(6)
–Mo(6)	3.182(6)	Li(2)–Mo(1)	3.743(6)
Li(3)–Mo(4)	3.208(6)	–Mo(1)	3.784(6)
–Mo(5)	3.229(6)	–Mo(3)	3.669(6)
Li(4)–Mo(10)	3.307(6)	–Mo(10)	3.844(6)
–Mo(12)	3.305(6)	Li(2′)–Mo(2)	3.762(6)
Li(4′)–Mo(7)	3.409(6)	Li(3)–Mo(3)	3.770(6)
–Mo(9)	3.381(6)	–Mo(3)	3.754(6)
		–Mo(1)	3.635(6)
		–Mo(7)	3.893(6)
		Li(3′)–Mo(4)	3.773(6)
		Li(4)–Mo(6)	3.635(6)
		–Mo(8)	3.540(6)
		–Mo(11)	3.749(6)
		Li(4′)–Mo(11)	3.748(6)

[a] Estimated standard deviations are given in parentheses.
[b] Primed and unprimed atoms are related by inversion.

tude have been noted previously for other molybdenum bronze structures.

In the V_2O_5-type layers, molybdenum ions are arranged in clusters of six (Fig. 4). Mo–Mo distances between corner-sharing octahedra along the *c* direction within these clusters (e.g., Mo(2)–Mo(6) or Mo(5)–Mo(4), Fig. 4, and related distances in Table III) are significantly larger than the corresponding distances between two clusters (e.g., Mo(6)–Mo(2′), etc.), an effect related to coulombic repulsion. Long Mo–Mo distances are associated with octahedra that edge share with molybdenum. In contrast, the shorter Mo–Mo′ distances are associated with octahedra that edge share with lithium.

The Mo–Mo distances are too long for metallic bonding in any direction. Indeed, the shortest Mo–Mo distance in the present structure (3.1648(3) Å) is longer than the longest (adjacent) Mo–Mo distance in typical molybdenum phases with strong metallic interactions (*14*). Along *c*, MoO_6 octahedra are connected by corner sharing to form infinite chains (Fig. 2a) and the Mo–O bond

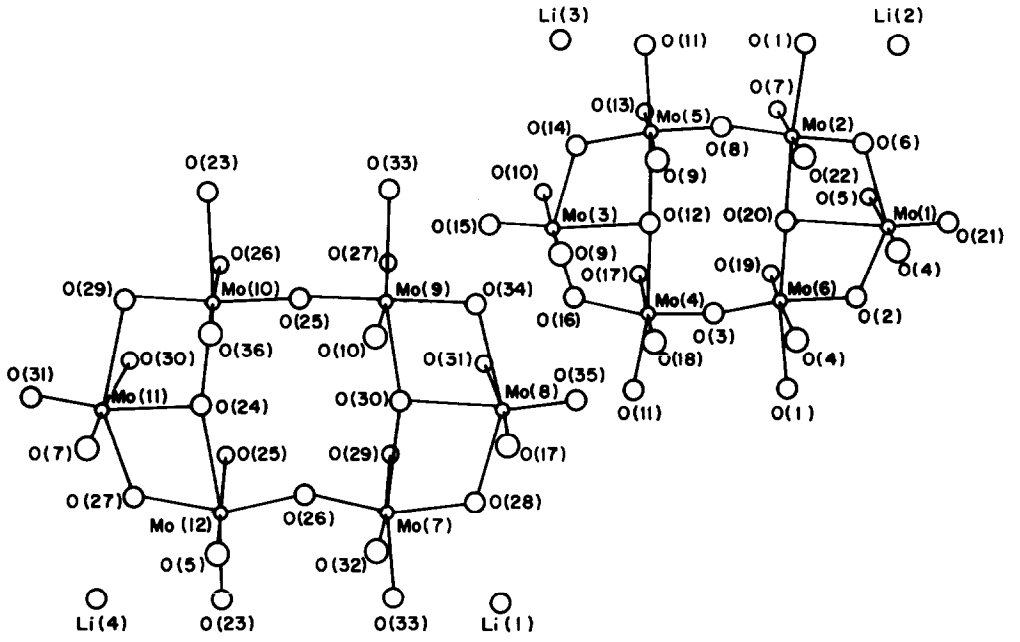

FIG. 3. ORTEP view approximately along b^* of the $Li_{0.33}MoO_3$ structure showing the atom numbering scheme for the unique ions. The c axis is approximately vertical.

distances are sufficiently short (1.861(2)–1.995(2) Å) for good Mo–O–Mo dt_{2g}-$p\pi$ orbital overlap. Hence, the highest electrical conductivity would be expected along this direction (*15*). Along b^*, there is a continuous Mo–O–Mo interaction arising from corner and edge sharing (Fig. 2b). In this case, however, the range of Mo–O distances is large (cf., Mo(9)–O(10), 1.666(2); Mo(9)–O(27), 2.400(2) Å) and some are too long for good orbital overlap (*15*). Therefore, the conductivity should be considerably lower along the b^* direction. Finally, the Mo–O–Mo interaction is not continuous along the [$\bar{3}$10] direction (Fig. 2a) and this should correspond to minimum conductivity.

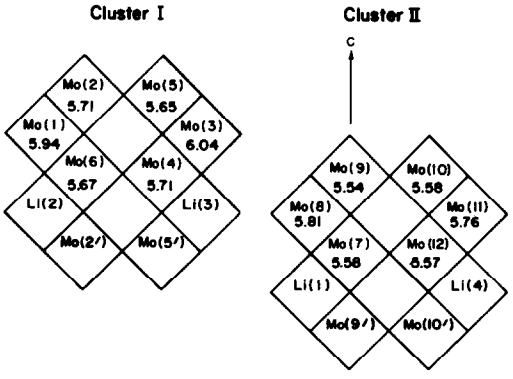

FIG. 4. Sketch of the two unique molybdenum clusters illustrating the Mo–Mo interactions. The valence of each molybdenum ion is also indicated.

Mo–O valences, s, calculated using the equation (*16*) $s = (d/d_0)^{-N}$, are shown in Table III. Here, d is the crystallographic interatomic distance, while d_0 and N are constants taken from the compilation of Brown (*16*). In the present work, values of $d_0 = 1.882$ Å and $N = 6.0$ were used. Li–O valences, calculated using the equation (*17*) $s = \exp[-(R - R_0)/B]$, where $R_0 = 1.292$ Å and $B = 0.48$, are also shown in Table III. For each molybdenum ion, there are one or two interactions of low order, and thus, the

net or effective coordination numbers of the molybdenum ions might more properly be regarded as four or five. The wide range of Mo–O distances in molybdenum oxide structures and the consequent difficulties associated with describing the coordination geometry have been noted previously (*3*). In the present structure, molybdenum sites involved in edge sharing with two adjacent molybdenum octahedra (e.g., the corner molybdenum ions Mo(1), Mo(3), Mo(8), and Mo(11) in Fig. 4) show two very strong Mo–O interactions (s = 1.53–1.92), two interactions of intermediate strength (0.84–1.12), and two very weak interactions (0.11–0.44). Thus, these molybdenum ions may be regarded as pseudo four-coordinate. Their coordination polyhedra most nearly correspond to four adjacent vertices of an octahedron with the metal near the center of a triangular face (i.e., a metal-centered octahedron with two *cis* sites vacant). In contrast, the remaining eight unique octahedra are more nearly pseudo five-coordinate with distorted square-pyramidal coordination geometry. They each show one strong interaction (1.88–2.10), four interactions of intermediate strength (0.57–1.07), and one very weak interaction (0.18–0.30). For each pseudo four-coordinate molybdenum, the weak interactions are approximately along b^* and $[\bar{3}10]$, while for the pseudo five-coordinate molybdenum atoms, they are all along b^*. In cluster II, which is linked to adjacent layers by corner and edge sharing, weak interactions occur along the edge-shared boundary between layers III and IV (Fig. 2b) such that the resulting pseudo four- and five-coordinate polyhedra all "point away" from this boundary. In cluster I, which is linked to adjacent layers exclusively by corner sharing, this directionality is not observed, and within a given cluster, two polyhedra point in a direction opposite to the remaining four.

The valence for each molybdenum ion is shown in Fig. 4. The average valence, 5.71, is quite close to the value of 5.67 expected for $Li_{0.33}MoO_3$. Molybdenum ions on cluster I show higher valences than those on cluster II. Thus, the less densely packed molybdenum ions (e.g., those linked to adjacent layers along b^* only by corner sharing) exhibit the higher valences, as might be expected from coulombic considerations. Within a given cluster, corner molybdenum ions (Mo(1), Mo(3), Mo(8), and Mo(11)) have the highest charge. The valence of corner-shared molybdenum ions along c are lower and are uniform within a given chain, providing additional evidence for good conductivity in this direction. Indeed, it is possible that $Li_{0.33}MoO_3$ is a metallic conductor along c. In any other direction, this material should be semiconducting, as has been previously observed (*5*).

It has been suggested that $Li_2Mo_4O_{13}$ is a precursor for the formation of $Li_{0.33}MoO_3$ (*5, 8, 9*). The crystal structure of both the high- and low-temperature polymorphs of $Li_2Mo_4O_{13}$ (*17, 18*) are derived from the V_6O_{13} (*18*) structure type. V_6O_{13}, in turn, is closely related to the V_2O_5 structure type (Fig. 1), the building block of $Li_{0.33}MoO_3$. This close structural relationship between $Li_2Mo_4O_{13}$ and $Li_{0.33}MoO_3$ may help explain why these two materials always appear to coexist in reaction ampoules.

The crystal structures of $K_{0.33}MoO_3$ (*3*) and $Cs_{0.33}MoO_3$ (*2*), the other known $M_{0.33}MoO_3$ phases, are of the layered type while $Li_{0.33}MoO_3$ is three-dimensional even though all three structures contain the six-octahedra molybdenum cluster (Fig. 4) as the basic building block. The difference in structure is probably related to the small size of the lithium ion which can fit easily into vacant octahedral oxygen sites. Similar effects of alkali ion size on crystal structure have been observed in the $M_2Mo_4O_{13}$ series (*18*).

Finally, we note that this work clearly establishes the structure and composition

of the triclinic, stoichiometric, lithium molybdenum bronze, $Li_{0.33}MoO_3(LiMo_3O_9)$. Further work will be required to determine the relationship of this phase to the monoclinic phase(s?) reported previously by other workers (see Introduction).

Acknowledgments

We thank W. H. McCarroll for providing suitable crystals of $Li_{0.33}MoO_3$. The work received support from the National Science Foundation—Solid State Chemistry Grant DMR-84-04003 and from the National Institutes of Health—Crystallographic Instrumentation Grant 1510 RRO 1486 01A1.

References

1. R. Brusetti, B. K. Chakraverty, J. Devenyi, J. Dumas, J. Marcus, and C. Schlenker, "Recent Developments in Condensed Matter Physics" (J. T. DeVreese, L. F. Lemmens, V. E. VanDoren, and J. VanRoyen, Eds.), Vol. 2 p. 181, Plenum, New York, 1982; J. P. Pauget, S. Kagoshima, C. Schlenker, and J. Marcus, *J. Phys. Lett.* **44,** L–113 (1983); J. Dumas and C. Schlenker, "Proceedings of the International Symposium on Non-Linear Transport and Related Phenomena in Inorganic Quasi-one Dimensional Conductors," Sapporo, Japan, 1983.
2. P. P. Tsai, J. A. Potenza, and M. Greenblatt, to be published.
3. N. C. Stephenson and A. D. Wadsley, *Acta Crystallogr.* **19,** 241 (1965).
4. G. H. Bouchard, Jr., J. Perlstein, and M. J. Sienko, *Inorg. Chem.* **6,** 1682 (1967).
5. P. Strobel and M. Greenblatt, *J. Solid State Chem.* **36,** 331 (1981).
6. J. Graham and A. D. Wadsley, *Acta Crystallogr.* **20,** 93 (1966).
7. J. M. Reau, C. Fouassier, and P. Hagenmuller, *J. Solid State Chem.* **1,** 326 (1970).
8. K. R. Nair, E. Wang, and M. Greenblatt, *J. Solid State Chem.* **55,** 193 (1984).
9. W. H. McCarroll and M. Greenblatt, *J. Solid State Chem.* **54,** 282 (1984).
10. H. F. Frazen, H. R. Shanks, and B. H. W. S. deJong, Natl. Bur. Std. Spec. Publ. Nr. 364, p. 41, 1972.
11. P. Main, S. J. Fiske, S. E. Hull, L. Lessinger, G. Germain, J.-P. Declercq, and M. M. Woolfson, "MULTAN 82. A System of Computer Programs for the Automatic Solution of Crystal Structures from X-ray Diffraction Data," Univ. of York, England and Louvain, Belgium, 1982.
12. The Enraf-Nonius Structure Determination Package, Enraf-Nonius, Delft, Holland (1983), was used for data collection, processing and structure solution
13. H. G. Bachman, F. R. Ahmed, and W. H. Barnes, *Zeit. Krist.* **115,** 110 (1961); A. Bystrom, K.-A. Wilhelmi, and O. Brotzen, *Acta Chem. Scand.* **4,** 1119 (1950).
14. See, for example, metallic MoO_2 in which short and long Mo–Mo distances of 2.5106 and 3.1118 Å alternate. B. G. Brandt and A. C. Skapski, *Acta Chem. Scand.* **21,** 661 (1967). Other examples are found in molybdenum cluster compounds. C. C. Torardi and J. C. Calabrese, *Inorg. Chem.* **23,** 3281 (1984); C. C. Torardi, C. Feckette, W. H. McCarroll, and F. J. Disalvo, *J. Solid State Chem.* **62,** 241 (1986); C. C. Torardi and R. E. McCarley, *Inorg. Chem.* **24,** 476 (1985).
15. G. Travaglini and P. Wachter, *Solid State Commun.* **47,** 217 (1983).
16. I. D. Brown, "Structure and Bonding in Crystals" (M. O'Keefe and A. Navrotsky, Eds.), Vol. II, p. 1, Academic Press, New York, 1981.
17. B. M. Gatehouse and B. K. Miskin, *J. Solid State Chem.* **15,** 274 (1975).
18. B. M. Gatehouse and B. K. Miskin, *J. Solid State Chem.* **9,** 247 (1974).